Negative Differential Resistance in Mono and Bilayer Graphene p-n Junctions

Gianluca Fiori, *Member, IEEE*

***Abstract*—In this letter, we study the electrical characteristics of monolayer and bilayer graphene p-n junctions through the self-consistent solution of the 2-D Poisson and Schrödinger equations within the Non-Equilibrium Green's Function (NEGF) formalism. Negative differential resistance is observed in both devices at room temperatures, which opens the possibility of exploiting graphene in analog electronics. An analytical expression, which is suitable for a fast exploration along the parameter space, is provided and compared against the tight-binding model, showing good agreement.**

***Index Terms*—Bilayer graphene, Esaki diodes, monolayer, NEGF, quantum tunneling.**

I. Introduction

THE APPEALING electrical properties of graphene, such as large carrier mobility, have triggered an important collective effort aimed at a good understanding of its electrical behavior. The lack of an energy gap is however the most limiting roadblock, which prevents graphene to be exploited in digital electronics, despite the huge efforts made up to now toward this direction.

Probably, the key for success passes through leveraging on what graphene can indeed offer, rather than on what researchers would like to obtain. The lack of a band gap is, for example, not an issue in analog electronics, where graphene transistors for radio-frequency applications have been recently demonstrated to have remarkable cutoff frequencies on the order of hundreds of gigahertz [1], [2].

Zero band gap can, in addition, be a remarkable property in band-to-band tunneling based devices such as in Esaki diodes [3], whose negative differential resistance (NDR) leads to a wide span of applications such as oscillators, fast switching logic, and low-power amplifiers, just to cite few [4].

NDR in graphene has been recently demonstrated by means of simulations in monolayer graphene devices when considering an ideal square potential barrier [5]–[7] or in bilayer graphene in the presence of a constant longitudinal electric field [8].

However, in order to clearly understand if NDR can indeed be achieved in realistic devices, more accurate models based on the self-consistent solution of the Poisson and Schrödinger equations have to be adopted.

To this purpose, we have focused our attention on highly doped p-n junctions based on monolayer and bilayer graphene, fully exploiting our open source code NanoTCAD ViDES [9].

We will demonstrate that both monolayer and bilayer graphene have I–V characteristics with NDR. An analytical expression for the current will be also provided showing good agreement with numerical results.

II. Results and Discussion

The Poisson equation is solved along the 2-D domain self-consistently with the Schrödinger equation within a p_z orbital basis set in the real space through the NEGF formalism. As experimentally demonstrated by Wang et al. [10], since depositing graphene on SiO_2 does not alter its electronic structures, we have assumed the same tight-binding parameters as those for the free-standing graphene flake. In particular, we have considered the in-plane and the out-of-plane carbon–carbon hopping parameters, i.e., $t = -2.7$ eV and $t_p = -0.35$ eV, respectively [11], [12].

Semi-infinite contacts have been considered at device ends, whereas the 2-D extension along the transversal direction has been taken into account through Bloch periodic boundary conditions.

The device structure is depicted in Fig. 1(a), where null Neumann conditions are imposed at the 2-D domain boundaries (see dashed line). The monolayer/bilayer graphene is embedded in a SiO_2 dielectric with a relative dielectric constant $\varepsilon_r = 3.9$ and with top and bottom oxide thicknesses equal to 10 nm: larger thicknesses have been verified to provide the same quantitative results. The doped reservoirs are 15 nm long. In order to mimic the charge due to ionized impurities in the doped reservoirs (positive for the cathode and negative for the anode), we have imposed a fixed charge in correspondence of the C atoms: the fraction of doping atoms on carbon atoms is defined as the molar fraction f.

In Fig. 1(b) and (c), we show the I–V characteristics of the monolayer and bilayer graphene abrupt p-n junctions for different values of f. As it is clearly shown, NDR can be observed in both devices, and the difference between the maximum and the minimum currents in the NDR interval increases with increasing doping concentrations. For the same geometry

Manuscript received June 18, 2011; accepted July 11, 2011. Date of publication August 29, 2011; date of current version September 28, 2011. This work was supported in part by the European Council Seventh Framework Program through the STREP project GRAND under Contract 215752 and in part by the Ministero dell'Istruzione, dell'Università e della Ricerca-Programmi di Ricerca di Rilevante Interesse Nazionale project titled "Modeling and simulation of graphene nanoribbon field-effect transistors for high-performance and low-power logic applications" under Prot. 2008S2CLJ9, via the IUNET consortium. The review of this letter was arranged by Editor M. Passlack.

The author is with the Dipartimento di Ingegneria dell'Informazione, Elettronica, Informatica, Telecomunicazioni, Università di Pisa, 56126 Pisa, Italy (e-mail: gfiori@mercurio.iet.unipi.it).

Color versions of one or more of the figures in this letter are available online at http://ieeexplore.ieee.org.

Digital Object Identifier 10.1109/LED.2011.2162392

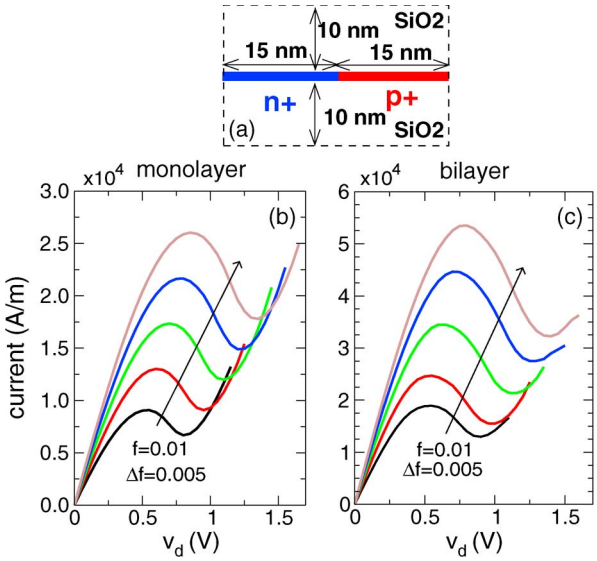

Fig. 1. (a) Sketch of the simulated device: the channel can be either monolayer or bilayer graphene. I–V characteristics of (b) monolayer and (c) bilayer graphene p-n junctions for different values of f. Each curve differs from the previous one by a difference in the molar fraction equal to $\Delta f = 5 \times 10^{-3}$.

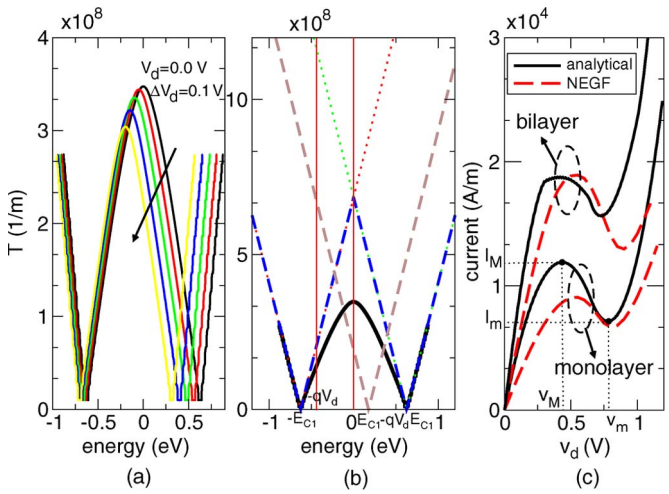

Fig. 2. (a) Transmission coefficient for different values of v_d. (b) Numerical and analytical transmission coefficients for $f = 0.01$; E_{C1} $(-E_{C1})$ is the potential deep in the anode (cathode) for $v_d = 0$ V, $-qv_d$ is the Fermi level of the anode, whereas the Fermi level of the cathode is fixed to zero. When applying v_d, the potential deep in the anode can be approximated by $E_{C1} - qv_d$. (c) I–V characteristics for monolayer and bilayer graphene diodes, obtained by means of NEGF and the analytical approach.

and the same f, a bilayer diode shows a current almost double compared with the monolayer counterpart.

The NDR and the qualitative trend of the diode characteristics can be kept by means of a simple analytical model.

In particular, in Fig. 2(a), the W-shaped transmission coefficient for a monolayer graphene diode is shown as a function of v_d, which is the anode-to-cathode bias. As it is shown, the minimum on the left (corresponding to the potential energy of the cathode) almost remains constant as a function of v_d, whereas the minimum on the right (corresponding to the anode) rigidly shifts by $-q\Delta v_d$, the v_d step applied to the anode, where q is the elementary charge.

At the Dirac point, energy dispersion in a monolayer graphene can be approximated by the relation $E = \hbar v_F |k|$, where $\hbar$ is the reduced Planck's constant, and v_F is the Fermi velocity $(v_F = 3a_{CC}t/2\hbar)$. It is then straightforward to demonstrate that the transmission coefficient for a constant potential reads

$$T_m(E) = \frac{2|E|}{\pi \hbar v_F}. \tag{1}$$

If E_{C1} $(-E_{C1})$ is the potential energy deep in the anode (cathode), assuming that the Fermi level of the cathode is equal to zero, and the Fermi level of the anode is equal to $-qv_d$, from the above considerations, the transmission coefficient can be approximated as

$$T_d(E) = \min\{T_m(E - E_{C1} + qv_d), T_m(E + E_{C1})\} \tag{2}$$

similarly to what was done in [13].

Fig. 2(b) shows the numerical (black solid line) and analytical (dashed lines) transmission coefficients.

As shown, for $|E| \geq |E_{C1}|$ (thermionic component), the numerical transmission coefficient matches the analytical one, whereas some discrepancies arise for $|E| < |E_{C1}|$ (tunneling component).

Applying the Landauer formula in the zero-temperature approximation, the current in the diode can be expressed as $i_d = (2q^2/h) \int_{-qv_d}^{0} T_d(E)\, dE$, which finally reads

$$i_d = \begin{cases} \frac{8q^2}{h^2 v_F} \frac{qv_d}{2} \left(-\frac{3}{2} qv_d + 2E_{C1}\right), & |qv_d| \leq |E_{C1}| \\ \frac{8q^2}{h^2 v_F} \left[\left(E_{C1} - \frac{qv_d}{2}\right)^2 + (qv_d - E_{C1})^2\right], & |qv_d| \geq |E_{C1}|, \end{cases} \tag{3}$$

where h is the Planck's constant.

From (3), one can easily obtain the minimum and the maximum of the current (I_m and I_M, respectively) and the corresponding v_d (v_m and v_M, respectively), as well as their difference

$$v_m = \frac{6}{5}\frac{E_{C1}}{q}; \quad v_M = \frac{2}{3}\frac{E_{C1}}{q}; \quad I_m = \frac{8q^2}{5h^2 v_F} E_{C1}^2$$

$$I_M = \frac{8q^2}{3h^2 v_F} E_{C1}^2; \quad I_M - I_m = \frac{16q^2}{15h^2 v_F} E_{C1}^2.$$

As shown in Fig. 2, the analytical model manages to reproduce the NDR, and it is in good agreement with numerical results obtained by means of tight-binding simulations, despite the simple linear energy dispersion approximation.

The simple analytical model can help in explaining the NDR behavior. i_d initially increases for low v_d. When further increasing v_d, the tunneling component of the current is suppressed, as demonstrated by the smaller area of the transmission coefficient within the energy range $[-E_{C1} : E_{C1} - qv_d]$. i_d finally follows the increasing monotonic behavior, when the thermionic component of the current becomes predominant, i.e., roughly for $qv_d > E_{C1}$.

The analytical model also reproduces the trend of the I–V characteristics for different molar fractions. In particular, the larger the molar fraction, the larger E_{C1} and the larger the difference $I_M - I_m$, as can be also observed in Fig. 1.

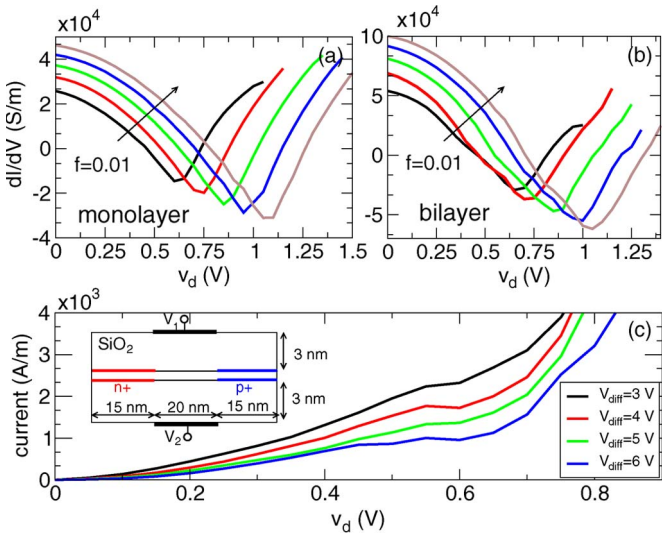

Fig. 3. Negative differential conductance as a function of v_d and for different values of f for the (a) monolayer and (b) bilayer diodes: curves differ by a molar fraction difference $\Delta f = 5 \times 10^{-3}$. (c) I–V characteristic of the bilayer graphene diode as a function of $V_{\rm diff}$; $V_1 = V_{\rm diff}/2 + v_d$ and $V_2 = -V_{\rm diff}/2 + v_d$. The transversal cross section is shown in the inset.

Same considerations follow for a bilayer graphene, where the transmission coefficient reads

$$T_b(E) = \frac{2\sqrt{2m^*E}}{\pi\hbar} \tag{4}$$

where m^* is the relative effective mass equal to 0.07, whereas the transmission coefficient can be expressed as in (2), where T_m is substituted by T_b. For the bilayer case, two bands have been taken into account, and the current has been numerically computed.

In Fig. 3(a) and (b), the differential conductance of the monolayer and bilayer graphene p-n junctions is shown for different molar fractions f, whereas in Fig. 3(c), we have shown the results for a bilayer p-n junction, whose transversal section is shown in the inset. In particular, here we want to investigate the impact of band-gap opening on the I–V characteristics through the application of a vertical electric field. In correspondence of doped regions, the potentials on the top and bottom graphene layers are pinned to the same value; therefore, in order to be effective, the electric field has to be applied over an undoped region, whose length has been taken equal to 20 nm. Two independent gates have been considered, and similarly to what was done in [12], they have been biased at $V_1 = V_{\rm diff}/2 + v_d$ and $V_2 = -V_{\rm diff}/2 + v_d$. As shown, inducing a band gap does not seem to be beneficial in increasing NDR, but rather detrimental for this particular configuration; this issue anyway needs further investigation, particularly through a deeper exploration along the device design space.

III. Conclusion

We have investigated the NDR in monolayer and bilayer graphene p-n junctions through numerical simulations. NDR appears in both diodes, and the peak-to-valley difference increases for increasing doping concentration of the reservoirs, as also predicted by a purposely devised analytical model. The current study then represents a demonstration that graphene can have potentials for analog electronics, and in particular for Esaki-like diodes, affordable by a state-of-the-art fabrication process. As a final remark, it is worth noticing that despite graphene p-n junction has already been experimentally demonstrated [14], [15], no NDR has been observed up to now. We believe that NDR can indeed be achieved when considering close and highly doped reservoirs; these are the hints we provide to the fabrication side.

References

[1] Y. Wu, Y.-M. Lin, A. A. Bol, K. A. Jenkins, F. Xia, D. B. Farmer, Y. Zhu, and P. Avouris, "High-frequency, scaled graphene transistors on diamond-like carbon," *Nature*, vol. 472, no. 7341, pp. 74–78, Apr. 2011.

[2] L. Liao, Y.-C. Lin, M. Bao, R. Cheng, J. Bai, Y. Liu, Y. Qu, K. L. Wang, Y. Huang, and X. Duan, "High-speed graphene transistors with a self-aligned nanowire gate," *Nature*, vol. 467, no. 7313, pp. 305–308, Sep. 2010.

[3] L. Esaki, "New phenomenon in narrow germanium p-n junctions," *Phys. Rev.*, vol. 109, no. 2, pp. 603–604, Jan. 1958.

[4] J. P. Sun, G. I. Haddad, P. Mazumder, and J. N. Schulman, "Resonant tunneling diodes: Models and properties," *Proc. IEEE*, vol. 86, no. 4, pp. 641–661, Apr. 1998.

[5] V. N. Do, A. V. H. Nguyen, P. Dollfus, and A. Bournel, "Electronic transport and spin-polarization effects of relativisticlike particles in mesoscopic graphene structures," *J. Appl. Phys.*, vol. 104, no. 6, pp. 063708-1–063708-7, Sep. 2008.

[6] D. Dragoman and M. Dragoman, "Negative differential resistance of electrons in graphene barrier," *Appl Phys Lett.*, vol. 90, no. 14, pp. 143111-1–143111-3, Apr. 2007.

[7] V. H. Nguyen, A. Bournel, C. Chassat, and P. Dollfus, "Quantum transport of Dirac fermions in graphene field effect transistors," in *Proc. SISPAD*, 2010, pp. 9–12.

[8] R. Nandkishore and L. Levitov, Interference under tunnel barrier and esaki-zener-type I–V characteristic in bilayer graphene p-n junctions, arXiv.

[9] [Online]. Available: http://www.nanohub.org/tools/vides

[10] Y. Wang, Z. Ni, T. Yu, Z. Shen, H. Wang, Y. Wu, W. Chen, and A. Wee, "Raman studies of monolayer graphene: The substrate effect," *J. Phys. Chem. C.*, vol. 112, pp. 10637–10640, 2008.

[11] G. Fiori and G. Iannaccone, "On the possibility of tunable-gap bilayer graphene," *IEEE Electron Device Lett.*, vol. 30, no. 3, pp. 261–264, Mar. 2009.

[12] G. Fiori and G. Iannaccone, "Ultralow-voltage bilayer graphene tunnel fet," *IEEE Electron Device Lett.*, vol. 30, no. 10, pp. 1096–1098, Oct. 2009.

[13] T. Low, S. Hong, J. Appenzeller, S. Datta, and M. S. Lundstrom, "Conductance asymmetry of graphene p-n junction," *IEEE Trans. Electron Devices*, vol. 56, no. 6, pp. 1292–1299, Jun. 2009.

[14] D. B. Farmer, Y.-M. Lin, A. Afzali-Ardakani, and P. Avouris, "Behavior of a chemically doped graphene junction," *Appl. Phys. Lett.*, vol. 94, no. 21, pp. 213106-1–213106-3, May 2009.

[15] J. R. Williams, T. Low, M. S. Lundstrom, and C. M. Marcus, "Gate-controlled guiding of electrons in graphene," *Nat. Nanotech.*, vol. 6, no. 4, pp. 222–225, Apr. 2011.